

Analysis of discretization errors in LES

By Sandip Ghosal¹

1. Motivation and objectives

All numerical simulations of turbulence (DNS or LES) involve some discretization errors. The integrity of such simulations therefore depend on our ability to quantify and control such errors. In the classical literature (see e.g. Chu 1978) on analysis of errors in partial differential equations, one typically studies simple linear equations (such as the wave equation or Laplace's equation). The qualitative insight gained from studying such simple situations is then used to design numerical methods for more complex problems such as the Navier-Stokes equations. Though such an approach may seem reasonable as a first approximation, it should be recognized that strongly nonlinear problems, such as turbulence, have a feature that is absent in linear problems. This feature is the simultaneous presence of a continuum of space and time scales. Thus, in an analysis of errors in the one dimensional wave equation, one may, without loss of generality, rescale the equations so that the dependent variable is always of order unity. This is not possible in the turbulence problem since the amplitudes of the Fourier modes of the velocity field have a continuous distribution. The objective of the present research is to provide some quantitative measures of numerical errors in such situations. Though the focus of this work is LES, the methods introduced here can be just as easily applied to DNS. Errors due to discretization of the time-variable are neglected for the purpose of this analysis.

2. Accomplishments

In this report, analytical expressions for the power spectra of errors due to the spatial discretization of the Navier-Stokes equations are derived. In § 2.1, an expression for the numerical error is presented as the sum of "finite-differencing", "aliasing", and "modeling" errors that have different origins. In § 2.2, expressions for the power spectra of the first two kinds of errors are derived as well as the corresponding expressions for the subgrid and total nonlinear terms. The essential tool that makes the derivation of such an analytical expression possible is the "joint-normal hypothesis" for turbulent velocities. The essential technique is identical to that used by Batchelor in his derivation of the pressure spectrum of turbulence from the energy spectrum (Batchelor 1951, 1953). These results are applied to the LES of turbulence in § 2.3 to obtain some measure of numerical errors in finite-difference schemes, which are increasingly being used in turbulence computations on flows with complex boundaries. This report summarizes the essential results, the details of the mathematical development will be presented elsewhere (Ghosal 1995 - henceforth referred to as "paper 1").

¹ Present address: CNLS (MS-B258), LANL, Los Alamos, NM 87545

2.1 Calculation of discretization errors

Any representation of the true velocity field in a turbulent flow on a finite grid is necessarily approximate. One must be careful to distinguish between errors due to the finiteness of the representation and the “discretization error” of a numerical scheme. In a numerical simulation, the velocity field at any time-step can be regarded as an element of a vector space with a finite number of dimensions (N) where N is the number of variables retained in the computation. This is an approximate representation in a subspace of the larger vector space that contains the true solution. The best possible approximation to the true solution in the subspace is the projection onto the subspace (in fact that is the definition of a projection operator — see e.g. Helmberg 1969). The “ideal” or “best approximation” to the Navier-Stokes operator in the finite subspace is that operator that ensures that the numerical solution remains “locked” to the projection of the true solution at all times as both vectors move around in their respective vector spaces. It may be shown (see paper 1) that this condition is achieved by spectral methods (or properly dealiased pseudo-spectral methods) in the absence of subgrid modeling errors. By “discretization error”, \mathbf{E} , of a numerical method we mean the deviation of the right hand side evaluated with the method from what would have been obtained if the right-hand side of the full Navier-Stokes equation were projected into the computational subspace. Thus, for a spectral method used in conjunction with an ‘exact’ subgrid model, $\mathbf{E} = 0$.

In order to evaluate the formal expression for the error \mathbf{E} , one needs to introduce a basis. The most advantageous choice is the 3D Fourier-basis since in Fourier space differentiations reduce to multiplication by wavevectors and numerical differentiation reduces to multiplication by modified wave vectors (see e.g. Vichnevetsky 1982). We now restrict our attention to flows in a periodic cubical box. Further, while considering finite-difference methods, the grid will be assumed uniform in every direction. Let $E_i(\mathbf{k})$ denote the components of \mathbf{E} in the Fourier-basis with $i = 1$ to 3 corresponding to the x , y , and z directions respectively. Then $E_i(\mathbf{k})$ can be written as

$$E_i(\mathbf{k}) = E_i^{(\text{FD})}(\mathbf{k}) + E_i^{(\text{alias})}(\mathbf{k}) + E_i^{(\text{model})}(\mathbf{k}). \quad (1)$$

The first term arises because of the inability of the finite-differencing operator, $\delta/\delta x_k$, to accurately compute the gradient of short-wavelength waves. We call this the “finite-differencing error.” It vanishes for a spectral method that can differentiate waves of all wavelengths exactly. The second term arises due to the method of computation of the nonlinear term by taking products in physical space on a discrete lattice. This is called the “aliasing error” and is well known in the literature on pseudo-spectral methods (Canuto *et al.* 1988, Rogallo 1981). The last term is the difference between the true subgrid force and that computed using a subgrid model. We call this the “modeling error”.

In the following analysis, the magnitude of the error \mathbf{E} will be characterized by statistical properties such as its power spectral density. Such statistical measures can be precisely defined only in the limit where the wavevector can assume a continuum rather than a discrete set of values. In physical space this implies that we

are considering the grid size Δ and some characteristic scale of turbulence λ fixed and taking the limit as the size of the box $L \rightarrow \infty$. In actual simulations, of course, the box size L is finite. However, L is taken much larger than Δ or λ so that smooth power spectra can be defined and computed statistical quantities are not changed when the box size is increased further. This ensures that the computed quantities are indistinguishable from the ideal limit, $L \rightarrow \infty$. For the purpose of theoretical analysis it is advantageous to take the limit $L \rightarrow \infty$ first rather than at the end of the computation. Thus, in the Fourier-basis, the exact solution will be characterized by a continuum of wave vectors $\mathbf{k} \in \mathbf{R}^3$ and the numerical solution will be characterized by the subset $\mathbf{k} \in \mathcal{B}$ where $\mathcal{B} \equiv [-k_x^{\max}, k_x^{\max}] \times [-k_y^{\max}, k_y^{\max}] \times [-k_z^{\max}, k_z^{\max}]$. We will assume for simplicity that the grid length Δ is the same in all three directions so that $k_x^{\max} = k_y^{\max} = k_z^{\max} = k_m = \pi/\Delta$. Further, we will consider the LES “filter-width” and the grid length to be identical. This condition will be relaxed in § 2.3.3. In the limit of infinite box size, the discrete Fourier transform and its inverse take the form (a factor of $L^3/8\pi^3$ is ‘absorbed’ in the definition of the transform)

$$\hat{\phi}(\mathbf{k}) = \frac{\Delta^3}{8\pi^3} \sum_{\mathbf{x}} \phi(\mathbf{x}) \exp(-i\mathbf{k} \cdot \mathbf{x}) \quad \phi(\mathbf{x}) = \int_{\mathcal{B}} d\mathbf{k} \hat{\phi}(\mathbf{k}) \exp(i\mathbf{k} \cdot \mathbf{x}) \quad (2)$$

where the summation is over all lattice points over the infinite cubic lattice of spacing Δ and the integration over wave space ranges over all vectors $\mathbf{k} \in \mathcal{B}$. The following useful identity is readily derived by taking the limit of infinite box size:

$$\frac{\Delta^3}{8\pi^3} \sum_{\mathbf{x}} \exp(i\mathbf{K} \cdot \mathbf{x}) = \sum_{\mathbf{a} \in \Lambda} \delta(\mathbf{K} - \mathbf{a}) \quad (3)$$

where ‘ δ ’ is the Dirac delta function, Λ is the set of wavevectors of the form $(2pk_m, 2qk_m, 2rk_m)$ where p, q and r are integers (positive, negative or zero), and \mathbf{K} is any vector (not necessarily restricted to \mathcal{B}). [This relation is familiar in solid state physics (see e.g. chapter 1, pg. 12 of Jones & March 1973) where the set Λ goes by the name “Reciprocal Lattice”.] When the lattice spacing $\Delta \rightarrow 0$, the summation over lattice points in (2) becomes an integral over space and the usual continuous Fourier-transform is recovered. In this limit, the right hand side of relation (3) becomes simply $\delta(\mathbf{K})$ and (3) reduces to the familiar expansion of the delta-function in terms of exponentials.

Let us first consider the effect of projecting the exact right-hand side of the Navier-Stokes equation onto the Fourier-basis with wavevector \mathbf{k} . The ‘ i th component’ is given by

$$-iP_{imn}(\mathbf{k}) \left[\int_{\mathcal{B}} \int_{\mathcal{B}} d\mathbf{k}' d\mathbf{k}'' \delta(\mathbf{k}' + \mathbf{k}'' - \mathbf{k}) \hat{u}_m(\mathbf{k}') \hat{u}_n(\mathbf{k}'') + \hat{\tau}_{mn}(\mathbf{k}) \right] - \nu k^2 \hat{u}_i(\mathbf{k})$$

where P_{imn} has its usual meaning (see e.g. Lesieur 1987) and $\hat{\tau}_{mn}$ is the exact subgrid stress in Fourier-space. The Einstein summation convention for tensor

indices is implied throughout this report except where otherwise noted. If the exact derivative operator $\partial/\partial x_k$ is replaced by the numerical differentiation $\delta/\delta x_k$, multiplication by wavevectors \mathbf{k} are replaced by multiplication by the corresponding modified wavevectors $\tilde{\mathbf{k}}$. Thus, we obtain

$$E_i^{(\text{FD})}(\mathbf{k}) = i \left[P_{imn}(\tilde{\mathbf{k}}) - P_{imn}(\mathbf{k}) \right] \int_{\mathcal{B}} \int_{\mathcal{B}} d\mathbf{k}' d\mathbf{k}'' \delta(\mathbf{k}' + \mathbf{k}'' - \mathbf{k}) \hat{u}_m(\mathbf{k}') \hat{u}_n(\mathbf{k}'') \quad (4)$$

$$+ i \left[P_{imn}(\tilde{\mathbf{k}}) \hat{T}_{mn}^M(\mathbf{k}) - P_{imn}(\mathbf{k}) \hat{\tau}_{mn}^M(\mathbf{k}) \right] + \nu(\tilde{k}^2 - k^2) \hat{u}_i(\mathbf{k}),$$

where $\hat{T}_{mn}^M(\mathbf{k})$ is the ‘‘modified subgrid model’’ obtained by replacing all multiplication by wavevectors (if any) in the subgrid model $\hat{\tau}_{mn}^M(\mathbf{k})$ by the corresponding multiplication by modified wavevectors.

To obtain the aliasing error, we consider the effect of evaluating the nonlinear term in physical space:

$$-i P_{imn}(\tilde{\mathbf{k}}) \left[\widehat{u_m(\mathbf{x})u_n(\mathbf{x})} + \hat{T}_{mn}^M(\mathbf{k}) \right].$$

On using the definition (2) of the discrete Fourier transform we have

$$\widehat{u_m(\mathbf{x})u_n(\mathbf{x})} = \frac{\Delta^3}{8\pi^3} \sum_{\mathbf{x}} u_m(\mathbf{x})u_n(\mathbf{x}) \exp(-i\mathbf{k} \cdot \mathbf{x}). \quad (5)$$

When $u_m(\mathbf{x})$ and $u_n(\mathbf{x})$ in (5) are expanded in the Fourier-basis we get

$$\widehat{u_m(\mathbf{x})u_n(\mathbf{x})} = \frac{\Delta^3}{8\pi^3} \sum_{\mathbf{x}} \int_{\mathcal{B}} \int_{\mathcal{B}} d\mathbf{k}' d\mathbf{k}'' \hat{u}_m(\mathbf{k}') \hat{u}_n(\mathbf{k}'') \exp[i(\mathbf{k}' + \mathbf{k}'' - \mathbf{k}) \cdot \mathbf{x}]. \quad (6)$$

The summation over lattice points can be performed using (3),

$$\widehat{u_m(\mathbf{x})u_n(\mathbf{x})} = \sum_{\mathbf{a} \in \Lambda} \int_{\mathcal{B}} \int_{\mathcal{B}} d\mathbf{k}' d\mathbf{k}'' \hat{u}_m(\mathbf{k}') \hat{u}_n(\mathbf{k}'') \delta(\mathbf{k}' + \mathbf{k}'' - \mathbf{k} - \mathbf{a}). \quad (7)$$

All the terms in the sum over $\mathbf{a} \in \Lambda$ with the exception of $\mathbf{a} = 0$ are clearly ‘‘spurious contributions’’ and constitute the ‘aliasing error’. Thus, we have

$$E_i^{(\text{alias})}(\mathbf{k}) = i P_{imn}(\tilde{\mathbf{k}}) \sum_{\mathbf{a} \in \Lambda_0} \int_{\mathcal{B}} \int_{\mathcal{B}} d\mathbf{k}' d\mathbf{k}'' \delta(\mathbf{k}' + \mathbf{k}'' - \mathbf{k} - \mathbf{a}) \hat{u}_m(\mathbf{k}') \hat{u}_n(\mathbf{k}'') + \delta \hat{T}_{mn}^M(\mathbf{k}) \quad (8)$$

where Λ_0 consists of the vectors $(2pk_m, 2qk_m, 2rk_m)$ where p, q and r can independently take on the values 0 or ± 1 but excluding the case $p = q = r = 0$. The reason integer values of p, q and r with modulus greater than 1 are not included in Λ_0 is that the relation $\mathbf{a} = \mathbf{k}' + \mathbf{k}'' - \mathbf{k}$ cannot be satisfied for such values if $\mathbf{k}, \mathbf{k}', \mathbf{k}'' \in \mathcal{B}$

and hence the delta function ensures that they do not contribute to the sum. The last term $\delta\hat{T}_{mn}^M(\mathbf{k})$ is the contribution to the aliasing error from the subgrid model. Obviously it depends on the nature of the model. For a subgrid model that uses a constant eddy viscosity, this term is linear in the resolved fields, and hence there is no contribution to the aliasing error. For more complicated models such as the Smagorinsky model, it is difficult to evaluate this contribution analytically due to the complicated nature of the nonlinearity.

The expressions (4) and (8) for the finite-differencing and aliasing errors involve the subgrid model τ_{ij}^M . Modeling errors associated with subgrid models are difficult to estimate, and, further, there is no obvious way to single out for this study any one among the wide variety of subgrid models in use. It is therefore advantageous to separate the issue of subgrid modeling from the issue of discretization errors which is the subject of this paper. In order to accomplish this, we introduce the concept of the “ideal subgrid model”:

$$\tau_{ij}^M = \tau_{ij}(\mathbf{x}, t) \quad (9)$$

where $\tau_{ij}(\mathbf{x}, t)$ is the exact subgrid stress. One might think of the “ideal subgrid model” (9) in the following way. Imagine a DNS with an infinitely greater resolution running concurrently with the given LES. At every time-step the exact subgrid stress is computed from the DNS fields and supplied to the LES simulation as a function of position. The rest of the analysis in this paper will be presented for such an idealized LES. Since τ_{ij}^M is already given as a function of position and time and involves no computation, it does not contribute to aliasing errors. Thus, for such an idealized LES, $\delta\hat{T}_{mn}^M = 0$ in (8). The contribution from the subgrid model is not, however, zero for the finite-differencing errors even for the ideal model (9). This is because the model is (inaccurately) differentiated for computing the pressure and the subgrid force. The subgrid terms in (4) for the ideal model (9) are given by $\hat{\tau}_{mn}^M = \hat{T}_{mn}^M = \hat{\tau}_{mn}$. Thus,

$$E_i^{(\text{FD})}(\mathbf{k}) = i \left[P_{imn}(\tilde{\mathbf{k}}) - P_{imn}(\mathbf{k}) \right] \iint dk' dk'' \delta(\mathbf{k}' + \mathbf{k}'' - \mathbf{k}) \hat{u}_m(\mathbf{k}') \hat{u}_n(\mathbf{k}'') \quad (10)$$

$$+ \nu(\tilde{k}^2 - k^2) \hat{u}_i(\mathbf{k}).$$

The integration in (10) now ranges over the entire wave-space. Clearly, for this ideal model

$$E_i^{(\text{model})}(\mathbf{k}) = iP_{imn}(\mathbf{k}) \left[\hat{\tau}_{mn}^{(M)}(\mathbf{k}) - \hat{\tau}_{mn}(\mathbf{k}) \right] = 0. \quad (11)$$

2.2 Power spectra

In this section, analytical expressions for the power spectra of the finite-differencing error, aliasing error, subgrid and total nonlinear term are derived.

2.2.1 Finite-differencing error

The power spectrum of the finite-differencing error is defined by $\mathcal{E}^{(\text{FD})}(k)$, where

$$\frac{\mathcal{E}^{(\text{FD})}(k)}{4\pi k^2} = \lim_{V \rightarrow \infty} \frac{8\pi^3}{V} \left\{ \langle E_i^{(\text{FD})}(\mathbf{k}) E_i^{(\text{FD})}(\mathbf{k})^* \rangle_{\Omega} \right\}, \quad (12)$$

$\langle \rangle_{\Omega}$ denotes angular average in wave-number space over the surface of the sphere $|\mathbf{k}| = k$ and V is the volume of the physical box containing the fluid.

From (4), we have,

$$\begin{aligned} \langle E_i^{\text{FD}}(\mathbf{k}) E_i^{\text{FD}}(\mathbf{k})^* \rangle = & \\ \Delta_{imn}(\mathbf{k}, \tilde{\mathbf{k}}) \Delta_{ipq}^*(\mathbf{k}, \tilde{\mathbf{k}}) \int d\mathbf{k}' d\mathbf{k}'' \langle \hat{u}_m(\mathbf{k}') \hat{u}_n(\mathbf{k} - \mathbf{k}') \hat{u}_p^*(\mathbf{k}'') \hat{u}_q^*(\mathbf{k} - \mathbf{k}'') \rangle & \\ + 2\nu \Im \left[i \Delta_{imn}^*(\mathbf{k}, \tilde{\mathbf{k}}) (\tilde{k}^2 - k^2) \int d\mathbf{k}' \langle \hat{u}_m^*(\mathbf{k}') \hat{u}_n^*(\mathbf{k} - \mathbf{k}') \hat{u}_i(\mathbf{k}) \rangle \right] & \\ + \nu^2 |\tilde{k}^2 - k^2|^2 \langle \hat{u}_i(\mathbf{k}) \hat{u}_i^*(\mathbf{k}) \rangle & \end{aligned} \quad (13)$$

where $\langle \rangle$ denotes ensemble average, $*$ denotes complex conjugate, \Im denotes the imaginary part, and $\Delta_{imn}(\mathbf{k}, \tilde{\mathbf{k}}) \equiv P_{imn}(\tilde{\mathbf{k}}) - P_{imn}(\mathbf{k})$. The following two properties of the Δ_{imn} tensors follow immediately from the corresponding properties of P_{imn} ; $\Delta_{imm} = 0$, $\Delta_{imn} = \Delta_{inm}$.

In order to make further analytical work possible with (13), we now introduce the ‘‘Millionshchikov hypothesis’’ (see e.g. Monin and Yaglom 1979) that in fully developed turbulence, the joint probability density function of any set of velocity components at arbitrary space-time points can be assumed to be joint-normal. The joint-normal hypothesis was originally evoked in turbulence in an attempt to close the hierarchy of equations for moments (see e.g. Lesieur 1987). Though this did not succeed, the joint-normal hypothesis has been successfully used in other contexts. Thus, Batchelor (Batchelor 1951) used it with success to predict the pressure spectrum of isotropic turbulence. The joint-normal hypothesis implies in particular

$$\begin{aligned} \langle u_i(\mathbf{x}_1) u_j(\mathbf{x}_2) u_k(\mathbf{x}_3) u_l(\mathbf{x}_4) \rangle = & \langle u_i(\mathbf{x}_1) u_j(\mathbf{x}_2) \rangle \langle u_k(\mathbf{x}_3) u_l(\mathbf{x}_4) \rangle \\ & + \langle u_i(\mathbf{x}_1) u_k(\mathbf{x}_3) \rangle \langle u_j(\mathbf{x}_2) u_l(\mathbf{x}_4) \rangle \\ & + \langle u_i(\mathbf{x}_1) u_l(\mathbf{x}_4) \rangle \langle u_j(\mathbf{x}_2) u_k(\mathbf{x}_3) \rangle \end{aligned} \quad (14)$$

and that all third order moments are zero. Here $\mathbf{u}(\mathbf{x}, t)$ is the true velocity field defined at all space time points. On taking the (continuous) Fourier transform of (14) and assuming the turbulence to be homogeneous, we have,

$$\begin{aligned} \langle \hat{u}_i(\mathbf{k}_1) \hat{u}_j(\mathbf{k}_2) \hat{u}_k(\mathbf{k}_3) \hat{u}_l(\mathbf{k}_4) \rangle = & \delta(\mathbf{k}_1 + \mathbf{k}_2) \delta(\mathbf{k}_3 + \mathbf{k}_4) \Phi_{ij}(\mathbf{k}_2) \Phi_{kl}(\mathbf{k}_4) \\ & + \delta(\mathbf{k}_1 + \mathbf{k}_3) \delta(\mathbf{k}_2 + \mathbf{k}_4) \Phi_{ik}(\mathbf{k}_3) \Phi_{jl}(\mathbf{k}_4) \\ & + \delta(\mathbf{k}_1 + \mathbf{k}_4) \delta(\mathbf{k}_2 + \mathbf{k}_3) \Phi_{il}(\mathbf{k}_4) \Phi_{jk}(\mathbf{k}_3), \end{aligned} \quad (15)$$

where Φ_{ij} is the Fourier transform of the correlation tensor $R_{ij}(\mathbf{x}_2 - \mathbf{x}_1) \equiv \langle u_i(\mathbf{x}_1) u_j(\mathbf{x}_2) \rangle$. On substituting (15) into (13) we get after some algebra (see paper 1)

$$\begin{aligned} \mathcal{E}^{\text{FD}}(k) = & \left\{ 8\pi k^2 \Delta_{imn}(\mathbf{k}, \tilde{\mathbf{k}}) \Delta_{ipq}^*(\mathbf{k}, \tilde{\mathbf{k}}) \int \Phi_{mp}^*(\mathbf{k}') \Phi_{nq}^*(\mathbf{k} - \mathbf{k}') d^3 \mathbf{k}' \right. \\ & \left. + \nu^2 |\tilde{k}^2 - k^2|^2 \Phi_{ii}(\mathbf{k}) \right\}_{\Omega}. \end{aligned} \quad (16)$$

Eq. (16) is the general result for homogeneous turbulence. If in addition, the turbulence is isotropic, Φ_{ij} simplifies (Batchelor 1953) to

$$\Phi_{ij}(\mathbf{k}) = \frac{E(k)}{4\pi k^4} (k^2 \delta_{ij} - k_i k_j) \quad (17)$$

where $E(k)$ is the three dimensional energy spectrum and δ_{ij} is the Kronecker-delta symbol. The integral in the first term of (16) may be written after substitution of (17) as

$$\begin{aligned} J_{mpnq}(\mathbf{k}) &\equiv 8\pi k^2 \int \Phi_{mp}^*(\mathbf{k}') \Phi_{nq}^*(\mathbf{k} - \mathbf{k}') d^3 \mathbf{k}' \\ &= \frac{k^2}{2\pi} \int \frac{E(P)E(Q)}{P^4 Q^4} [P^2 Q^2 \delta_{mp} \delta_{nq} - P_m P_p Q^2 \delta_{nq} - Q_n Q_q P^2 \delta_{mp} + P_m P_p Q_n Q_q] \\ &\quad \times \delta(\mathbf{P} + \mathbf{Q} - \mathbf{k}) d^3 \mathbf{P} d^3 \mathbf{Q}. \end{aligned} \quad (18)$$

This integral can be simplified (see paper 1). The result is

$$\begin{aligned} J_{mpnq}(\mathbf{k}) &= F_1(k) \delta_{mp} \delta_{nq} + F_2(k) (\delta_{mn} \delta_{pq} + \delta_{pn} \delta_{mq}) \\ &\quad + F_3(k) \left[\frac{k_m k_p}{k^2} \delta_{nq} + \frac{k_n k_q}{k^2} \delta_{mp} \right] + F_4(k) \frac{k_m k_p k_n k_q}{k^4} \end{aligned} \quad (19)$$

where

$$\begin{aligned} F_1(k) &= \frac{1}{16} [7I_4 + 6I_3 - 2I_2 + 5I_1] \\ F_2(k) &= \frac{1}{16} [-3I_4 + 2I_3 + 2I_2 - I_1] \\ F_3(k) &= \frac{1}{16} [-15I_4 - 6I_3 + 2I_2 + 3I_1] \\ F_4(k) &= \frac{1}{16} [45I_4 - 30I_3 - 6I_2 + 7I_1]. \end{aligned} \quad (20)$$

The terms I_m are defined as

$$I_m = k \int_0^\infty d\xi \int_{|\xi-1|}^{\xi+1} d\eta E(k\xi) E(k\eta) W_m(\xi, \eta) \quad (21)$$

where the weights W_m are defined as follows:

$$\begin{aligned} W_1(\xi, \eta) &= \frac{1}{\xi\eta} \\ W_2(\xi, \eta) &= \frac{(1 - \xi^2 - \eta^2)^2}{4\xi^3\eta^3} \\ W_3(\xi, \eta) &= \frac{(1 + \xi^2 - \eta^2)^2}{4\xi^3\eta} \\ W_4(\xi, \eta) &= \frac{[1 - (\xi^2 - \eta^2)^2]^2}{16\xi^3\eta^3}. \end{aligned} \quad (22)$$

Therefore, after substituting (19) in (16) and using the properties $\Delta_{imm} = 0$ and $\Delta_{imn} = \Delta_{inm}$, the following expression is obtained for the power spectrum of the finite-differencing error (no summation over repeated indices!):

$$\begin{aligned} \mathcal{E}^{(\text{FD})}(k) = & [F_1(k) + F_2(k)] \left\{ \sum_{i,m,n} |\Delta_{imn}(\mathbf{k}, \tilde{\mathbf{k}})|^2 \right\}_{\Omega} + 2F_3(k) \left\{ \sum_{i,m,n,p} \frac{k_m k_p}{k^2} \Delta_{imn}(\mathbf{k}, \tilde{\mathbf{k}}) \Delta_{ipn}^*(\mathbf{k}, \tilde{\mathbf{k}}) \right\}_{\Omega} \\ & + F_4(k) \left\{ \sum_{i,m,n,p,q} \frac{k_m k_p k_n k_q}{k^4} \Delta_{imn}(\mathbf{k}, \tilde{\mathbf{k}}) \Delta_{ipq}^*(\mathbf{k}, \tilde{\mathbf{k}}) \right\}_{\Omega} + 2\nu^2 E(k) \left\{ |\tilde{k}^2 - k^2|^2 \right\}_{\Omega} \end{aligned} \quad (23)$$

In (23), the functions $F_1(k)$, $F_2(k)$, $F_3(k)$ and $F_4(k)$ are known once the energy spectrum is specified. They are not affected by the choice of numerical schemes. On the other hand, the coefficients of these functions in (23) depend *only* on the numerical method (through the dependence of $\tilde{\mathbf{k}}$ on \mathbf{k}) and are quite independent of the physical spectrum. Thus, given a specific numerical scheme and energy spectrum, (23) can be used to compute the power spectrum of the finite-differencing error. This is done in §2.3 for various representative numerical schemes.

2.2.2 Aliasing errors

The power spectrum of the aliasing error is defined by

$$\frac{\mathcal{E}^{(\text{alias})}(k)}{4\pi k^2} = \lim_{V \rightarrow \infty} \frac{8\pi^3}{V} \left\{ \langle E_i^{(\text{alias})}(\mathbf{k}) E_i^{(\text{alias})}(\mathbf{k})^* \rangle \right\}. \quad (24)$$

From (8) one obtains

$$\begin{aligned} \langle E_i^{(\text{alias})}(\mathbf{k}) E_i^{(\text{alias})}(\mathbf{k})^* \rangle = & P_{imn}(\tilde{\mathbf{k}}) P_{ipq}^*(\tilde{\mathbf{k}}) \sum_{\mathbf{a}, \mathbf{a}' \in \Lambda_0} \int_{\mathcal{B}} \int_{\mathcal{B}} \int_{\mathcal{B}} \int_{\mathcal{B}} d\mathbf{k}_1 d\mathbf{k}_2 d\mathbf{k}_3 d\mathbf{k}_4 \\ & \times \langle \hat{u}_m(\mathbf{k}_1) \hat{u}_n(\mathbf{k}_2) \hat{u}_p^*(\mathbf{k}_3) \hat{u}_q^*(\mathbf{k}_4) \rangle \delta(\mathbf{k} + \mathbf{a} - \mathbf{k}_1 - \mathbf{k}_2) \delta(\mathbf{k} + \mathbf{a}' - \mathbf{k}_3 - \mathbf{k}_4). \end{aligned} \quad (25)$$

On applying the joint-normal hypothesis, (15), one gets after some algebra (see paper 1)

$$\begin{aligned} \mathcal{E}^{(\text{alias})}(k) = & 8\pi k^2 \sum_{\mathbf{a} \in \Lambda_0} \left\{ P_{imn}(\tilde{\mathbf{k}}) P_{ipq}^*(\tilde{\mathbf{k}}) \int_{\mathcal{B}} \int_{\mathcal{B}} d\mathbf{k}' d\mathbf{k}'' \Phi_{mp}^*(\mathbf{k}') \Phi_{nq}^*(\mathbf{k}'') \delta(\mathbf{k} + \mathbf{a} - \mathbf{k}' - \mathbf{k}'') \right\}_{\Omega}. \end{aligned} \quad (26)$$

The integral in (26) is difficult to handle analytically because integration over the cubical region \mathcal{B} destroys the spherical symmetry of the problem exploited in the computation of $\mathcal{E}^{\text{FD}}(k)$ in the last section. In order to make analytical progress, the following approximation is introduced. The region \mathcal{B} , which is a cube in \mathbf{k} -space,

is replaced by the largest sphere contained in it. Clearly, this procedure can be implemented simply by removing the suffix 'B' from the integral signs in (26) and replacing the energy spectrum $E(k)$ by

$$E^{\min}(k) = \begin{cases} E(k) & \text{if } k < k_m \\ 0 & \text{otherwise.} \end{cases} \quad (27)$$

The superscript 'min' indicates that this procedure underestimates the true aliasing error by failing to take account of the contribution of modes close to the eight corners of the cube. An alternative method that overestimates the error can be provided by replacing the cube by the smallest sphere that contains it. To obtain this estimate one needs to use in place of E^{\min} the following spectrum;

$$E^{\max}(k) = \begin{cases} E(k) & \text{if } k < \sqrt{3}k_m \\ 0 & \text{otherwise.} \end{cases} \quad (28)$$

The true aliasing error is then expected to lie between these two bounds. With the approximation so described, and with the energy spectrum defined as in (27) or (28), the integral in (26) may be extended to the entire wave space. Thus, one obtains

$$\mathcal{E}^{(\text{alias})}(k) = \sum_{\mathbf{a} \in \Lambda_0} \left\{ P_{imn}(\tilde{\mathbf{k}}) P_{ipq}^*(\tilde{\mathbf{k}}) J_{mpnq}(\mathbf{k} + \mathbf{a}) \right\}_{\Omega}. \quad (29)$$

Substitution of the expression for J_{mpnq} gives (no summation over repeated indices!):

$$\begin{aligned} \mathcal{E}^{(\text{alias})}(k) = \sum_{\mathbf{a} \in \Lambda_0} \left\{ [F_1(K) + F_2(K)] \sum_{i,m,n} |P_{imn}(\tilde{\mathbf{k}})|^2 \right. \\ \left. + 2F_3(K) \sum_{i,m,n,p} \frac{K_m K_p}{K^2} P_{imn}(\tilde{\mathbf{k}}) P_{ipn}^*(\tilde{\mathbf{k}}) + F_4(K) \sum_{i,m,n,p,q} \frac{K_m K_p K_n K_q}{K^4} P_{imn}(\tilde{\mathbf{k}}) P_{ipq}^*(\tilde{\mathbf{k}}) \right\}_{\Omega} \end{aligned} \quad (30)$$

where $\mathbf{K} = \mathbf{k} + \mathbf{a}$. Note that in this case the $F_i(K)$ does depend on the direction of \mathbf{k} so that the $F_i(K)$ cannot be extracted from the $\{ \}_{\Omega}$ operation. Though the summation over the set Λ_0 consists of $3^3 - 1 = 26$ terms, for a cubical box one only needs to evaluate 3 terms due to symmetry. Indeed, the full set of "aliasing modes", $\mathbf{a} \in \Lambda_0$, fall into three classes (Rogallo 1981):

$$3D \{(\pm 2k_m, \pm 2k_m, \pm 2k_m)\} \quad 2D \begin{cases} (\pm 2k_m, \pm 2k_m, 0) \\ (\pm 2k_m, 0, \pm 2k_m) \\ (0, \pm 2k_m, \pm 2k_m) \end{cases} \quad 1D \begin{cases} (\pm 2k_m, 0, 0) \\ (0, \pm 2k_m, 0) \\ (0, 0, \pm 2k_m) \end{cases}. \quad (31)$$

By symmetry all the contributions within each class are equal. Therefore,

$$\mathcal{E}^{(\text{alias})}(k) = 6\mathcal{E}_{1D}^{(\text{alias})}(k) + 12\mathcal{E}_{2D}^{(\text{alias})}(k) + 8\mathcal{E}_{3D}^{(\text{alias})}(k) \quad (32)$$

where $\mathcal{E}_{1D}^{(\text{alias})}(k)$ is the contribution from any one of the 1D modes, $\mathcal{E}_{2D}^{(\text{alias})}(k)$ is the contribution from any one of the 2D modes, and $\mathcal{E}_{3D}^{(\text{alias})}(k)$ is the contribution from any one of the 3D modes respectively. If the modified wave-number, $\tilde{\mathbf{k}}$, of a numerical method and the energy spectrum of the turbulence, $E(k)$, are known, (32) may be evaluated numerically using either $E^{\min}(k)$ or $E^{\max}(k)$ to get the lower and upper estimates for the aliasing error respectively.

2.2.3 Subgrid and total contributions

The total nonlinear term \mathbf{N} and the (exact) subgrid force \mathbf{S} can be readily written down in terms of the Fourier-basis:

$$N_i(\mathbf{k}) = -iP_{imn}(\mathbf{k}) \int d\mathbf{k}' d\mathbf{k}'' \delta(\mathbf{k}' + \mathbf{k}'' - \mathbf{k}) \hat{u}_m(\mathbf{k}') \hat{u}_n(\mathbf{k}''), \quad (33)$$

and

$$S_i(\mathbf{k}) = -iP_{imn}(\mathbf{k}) \left(\int \int_{\mathcal{B}} - \int_{\mathcal{B}} \int_{\mathcal{B}} \right) d\mathbf{k}' d\mathbf{k}'' \delta(\mathbf{k}' + \mathbf{k}'' - \mathbf{k}) \hat{u}_m(\mathbf{k}') \hat{u}_n(\mathbf{k}''). \quad (34)$$

The power-spectra are defined as

$$\frac{\mathcal{S}(k)}{4\pi k^2} = \lim_{V \rightarrow \infty} \frac{8\pi^3}{V} \{ \langle S_i(\mathbf{k}) S_i(\mathbf{k})^* \rangle \}_\Omega \quad (35)$$

$$\frac{\mathcal{N}(k)}{4\pi k^2} = \lim_{V \rightarrow \infty} \frac{8\pi^3}{V} \{ \langle N_i(\mathbf{k}) N_i(\mathbf{k})^* \rangle \}_\Omega \quad (36)$$

where $\{ \}_\Omega$ as usual denotes angular average over the sphere $|\mathbf{k}| = k$.

The evaluation of (36) is similar to the calculation of $\mathcal{E}^{\text{FD}}(k)$ in § 2.2.1. One only needs to replace ' Δ_{imn} ' in (16) by ' $-P_{imn}$ ' and drop the last term involving the viscosity. The resulting expressions can be further simplified using the properties of the P_{imn} tensors (see paper 1):

$$\mathcal{N}(k) = k^2 [F_1(k) + F_2(k) + F_3(k)]. \quad (37)$$

where F_1 , F_2 and F_3 are as defined in (20).

The computation of $\mathcal{S}(k)$ once again requires us to restrict the \mathbf{k} space integration to a cubical domain which makes it difficult to handle the integrals analytically. This difficulty is dealt with in precisely the same manner as was done in the computation of the aliasing error. The cubical domain in \mathbf{k} space is replaced by a spherical region of appropriate size. This is completely equivalent to replacing the energy spectrum $E(k)$ by a pseudo-spectrum $\tilde{E}^{\min}(k)$ or $\tilde{E}^{\max}(k)$ defined as:

$$\tilde{E}^{\min}(k) = \begin{cases} E(k) & \text{if } k > \sqrt{3}k_m \\ 0 & \text{otherwise} \end{cases} \quad (38)$$

and

$$\tilde{E}^{\max}(k) = \begin{cases} E(k) & \text{if } k > k_m \\ 0 & \text{otherwise.} \end{cases} \quad (39)$$

With this modification, the calculation is exactly identical to that just presented for the nonlinear term. Thus, one obtains

$$\mathcal{S}(k) = k^2 [F_1(k) + F_2(k) + F_3(k)]. \quad (40)$$

where in the evaluation of the functions F_i , the pseudo-spectrum $\tilde{E}^{\min}(k)$ or $\tilde{E}^{\max}(k)$ should be used in place of $E(k)$ to obtain the lower and upper bounds respectively.

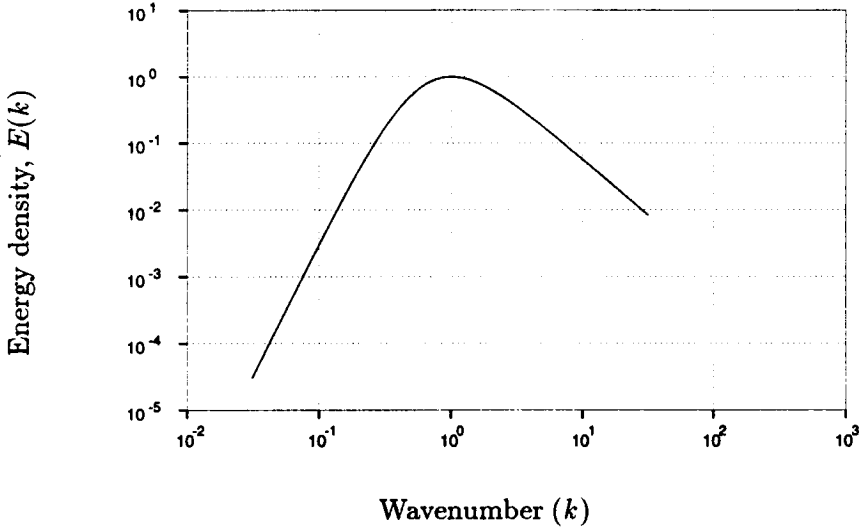


FIGURE 1. The Von-Karman spectrum normalized so that the maximum energy density is at $k = 1$ and $E(1) = 1$.

2.3 Application to LES

The results established in the previous sections will now be applied to establish quantitative measures of errors in LES. In LES, the grid spacing Δ is typically much larger than the Kolmogorov length so that molecular viscosity plays a negligible role. Therefore ‘ ν ’ is set to zero throughout this section. For the energy spectrum we assume the “Von-Karman form”

$$E(k) = \frac{ak^4}{(b + k^2)^{17/6}} \quad (41)$$

where the constants $a = 2.682$ and $b = 0.417$ are chosen so that the maximum of $E(k)$ occurs at $k = 1$ and the maximum value $E(1) = 1$. This can always be ensured by a proper choice of length and time-scales. The Von-Karman spectrum has the property $E(k) \sim k^4$ as $k \rightarrow 0$ and $E(k) \sim k^{-5/3}$ as $k \rightarrow \infty$ and is a fair representation of inertial range turbulence. A plot of this spectrum is shown in Fig. 1.

2.3.1 Spectra

The power spectra $\mathcal{N}(k)$ and $\mathcal{S}(k)$ are evaluated numerically from (37) and (40), respectively, using the Von-Karman spectrum. We assume the LES filter to be equal to the grid spacing Δ . The results are shown in Fig. 2 for $k_m = 8$ and 32, where $k_m \equiv \pi/\Delta$. It is seen that the power spectrum of the total nonlinear term is reasonably flat at high wavenumbers while the subgrid contribution rises monotonically to a maximum (which appears as a “cusp” when plotted on a linear

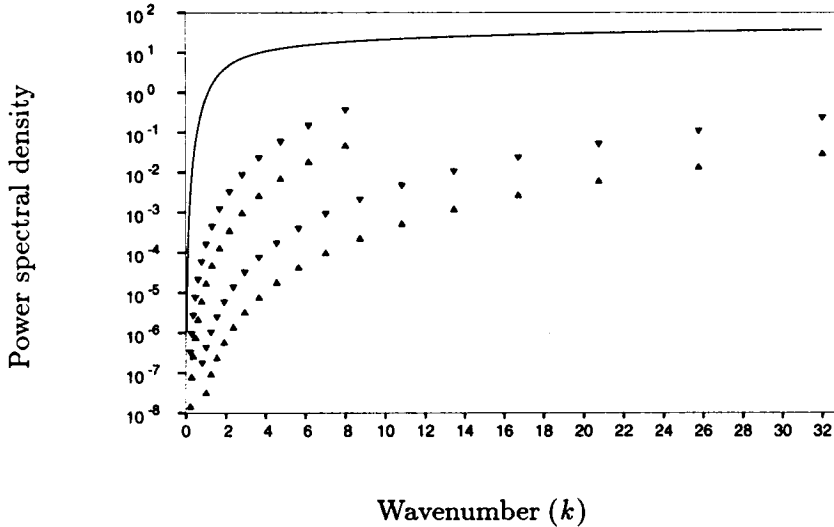


FIGURE 2. The total nonlinear term (—) compared to the lower (▲) and upper (▼) bound of the true subgrid force for $k_m = 8$ and 32.

scale) at the cut-off wavenumber k_m . The subgrid contribution is seen to be a relatively small part of the total contribution from the nonlinear term.

Subgrid modeling is a very important part of large-eddy simulation. A parametrization of the interaction of the unresolved eddies with the resolved ones is expressed as a subgrid model. It is therefore desirable that the errors inherent in the numerical method be much smaller than the physically motivated subgrid model. We now examine to what extent such an expectation is realized for a second order central-difference method implemented with the nonlinear term in divergence form. A second order central-difference scheme is characterized by the modified wavenumber $\bar{k}_i = \sin(k_i \Delta) / \Delta$ ($i = 1, 2$ or 3). Eq. (23) is used to compute the power spectra of the finite-differencing error $\mathcal{E}^{(FD)}(k)$ for $k_m = 8$ and 32. These results are compared to the power spectra of the respective subgrid terms in Fig. 3. Only two values of k_m are shown for clarity. The figures have the same qualitative appearance for all values of k_m . The power spectrum of the finite-differencing error rises to a maximum at $k = k_m$ in the same manner as the subgrid contribution. However, for all values of k_m the finite-differencing error is substantially larger than the subgrid contribution over the entire wavenumber range.

Figure 3 indicates that the error in a second order scheme cannot be reduced to a level below the subgrid contribution by sufficiently refining the grid. As the grid is refined (k_m is increased), both the error as well as the subgrid force decrease for all wavenumbers. However, the error continues to dominate the subgrid force throughout the wavenumber range irrespective of the resolution. Let us now examine if this situation can be improved by using higher order central-difference schemes. Figure 4 shows the finite-differencing error evaluated using (23) for a second, fourth,

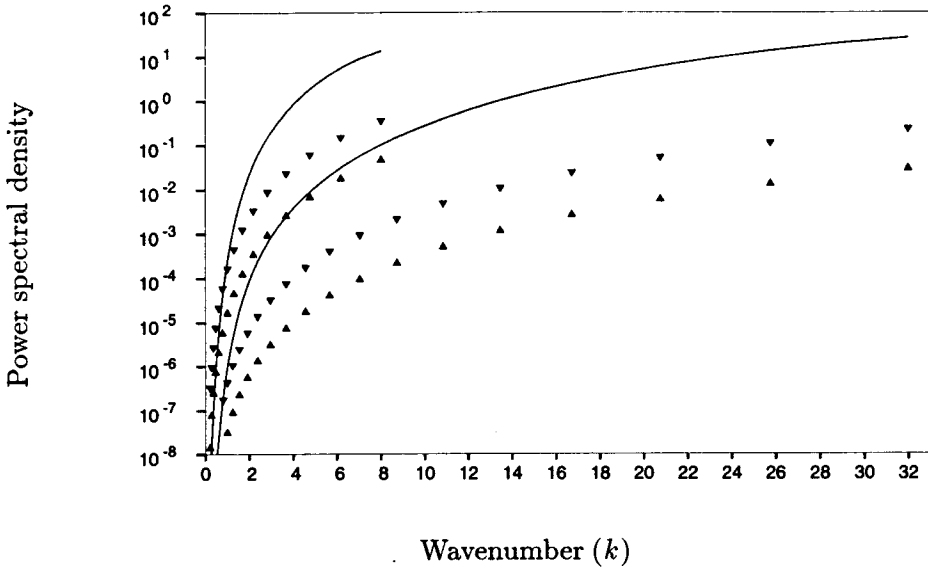


FIGURE 3. Finite-differencing error for the second order central-difference scheme (—) compared to the lower (▲) and upper (▼) bounds of the true subgrid force for $k_m = 8$ and 32.

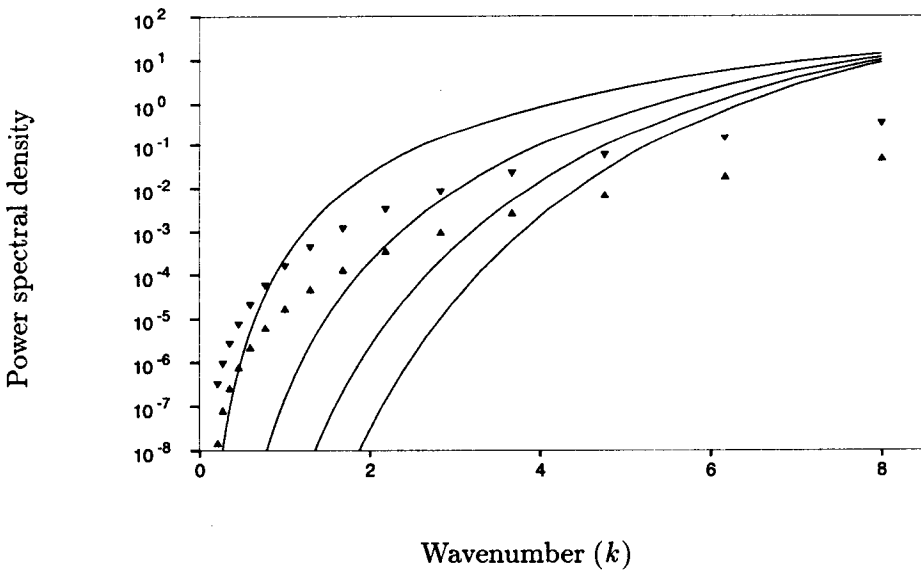


FIGURE 4. Finite-differencing errors (—) compared to the lower (▲) and upper (▼) bounds of the subgrid force for $k_m = 8$. The numerical schemes considered are second (highest curve), fourth, sixth, and eighth (lowest curve) order central-differences.

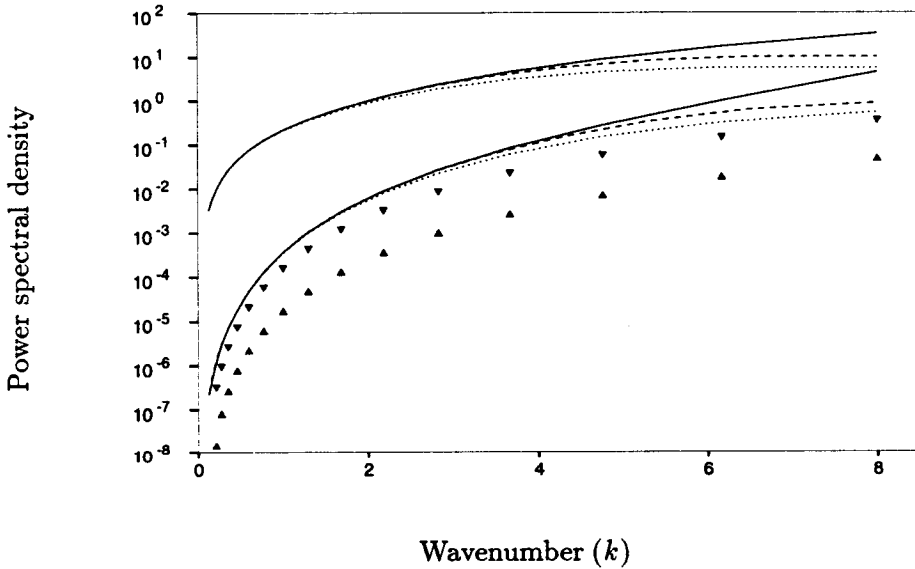


FIGURE 5. The aliasing error for a second-order central-difference method ($\cdots\cdots$), a fourth-order central-difference method ($- - -$) and an undealiased pseudo-spectral method ($—$), compared to the lower (\blacktriangle) and upper (\blacktriangledown) bounds of the subgrid force. Each method is represented by a pair of curves corresponding to the lower and upper bounds of the error.

sixth, and eighth order central-difference scheme together with the subgrid term, computed using (40) for a fixed resolution, $k_m = 8$. It is seen that higher order schemes do lead to reduced levels of error. However, even with an eighth order scheme, the subgrid contribution is dominated by numerical errors in about half of the wavenumber range.

Figure 5 shows the corresponding comparison for the aliasing error computed using (30). In general, increasing the order of a scheme has a relatively weak effect on the aliasing error and the effect is primarily in the high wavenumber region. This effect is in fact in the “reverse” direction compared to the finite-differencing error. That is, the lowest pair of curves which correspond to a second-order scheme have the smallest aliasing error and the highest pair corresponding to an undealiased pseudo-spectral method have the largest. The aliasing errors for sixth and eighth order schemes are intermediate between the fourth and the pseudo-spectral; they have been omitted from Fig. 5 for clarity. The effect is of course quite easy to understand. In the one dimensional problem, the aliasing part of the nonlinear term is multiplied by the modified wavenumber which approaches zero at the cut-off so that the aliasing error is also reduced to zero at k_m . In the three dimensional problem a similar situation applies except that the power spectrum does not actually go to zero on account of the averaging over wavenumber shells. However, the aliasing error is reduced at high wavenumbers for central-difference schemes.

2.3.2 Scaling laws

In this section, the dependence of some measure of “global error” on resolution, k_m , is investigated. An appropriate measure of the kind is

$$\sigma_* = \left[\int_0^{k_m} \mathcal{E}^{(*)}(k) dk \right]^{1/2} \quad (42)$$

where ‘*’ stands for ‘FD’, ‘alias’, ‘nl’ or ‘sg’ corresponding to the global finite-differencing error, aliasing error, total nonlinear term, or subgrid term respectively. σ_* is closely related but not exactly equal to the rms value, which is given by the integral of the power spectrum over the entire wavenumber range. The correspondence is not exact because the modes at the corners of the cube $[-k_m, k_m] \times [-k_m, k_m] \times [-k_m, k_m]$ outside of the inscribed sphere of radius k_m have not been included in the definition (42). Thus, σ_* is a lower bound of the true rms value. The σ_* can be evaluated as a function of k_m by numerically integrating the power spectra $\mathcal{E}^{(*)}(k)$ presented earlier.

Figure 6 shows the lower and upper bounds (measured by the corresponding σ_*) for the subgrid force σ_{sg} as a function of k_m . The corresponding quantity for the total nonlinear term σ_{nl} is also shown for comparison. The subgrid contributions are seen to obey a power law. A least square fit gives

$$\sigma_{sg} = \begin{cases} 0.36 k_m^{0.39} & \text{(Lower bound)} \\ 0.62 k_m^{0.48} & \text{(Upper bound)} \end{cases} \quad (43)$$

The total nonlinear term also appears to follow a power law. A least square fit in this case gives

$$\sigma_{nl} = 1.04 k_m^{0.97}. \quad (44)$$

The fitted curves (43) and (44) are shown in Fig. 6 as dashed and solid lines respectively. Thus, the relative subgrid contribution is (roughly) $\sigma_{sg}/\sigma_{nl} \sim k_m^{-0.5}$, that is, the role of the subgrid model decreases at higher resolution. As an illustration, for an LES that resolves about a decade of scales beyond the energy peak, the rms value of the subgrid force, according to this formula, should be in the approximate range 11 – 19 % of the rms value of the total force.

The following heuristic “derivation” (Tennekes & Lumley 1983) is sometimes given for the scaling of the subgrid term. The traceless subgrid stress is $\tau_{ij} = 2\nu_t S_{ij}$ where ν_t is the eddy-viscosity and S_{ij} is the rate of strain. The rate of dissipation $\epsilon = \tau_{ij} S_{ij} = \nu_t |S|^2$ is a constant according to the classical Kolmogorov argument. Therefore, $|\tau_{ij}| \sim \nu_t |S| \sim \sqrt{\epsilon \nu_t}$. Now, it seems reasonable to postulate that ν_t is the product of the grid-spacing, Δ , and the rms velocity of the subgrid eddies, $\sqrt{\langle u'^2 \rangle}$. The latter can be estimated from the Kolmogorov spectrum

$$\sqrt{\langle u'^2 \rangle} \sim \left[\int_{k_m}^{\infty} E(k) dk \right]^{1/2} \sim \left[\int_{k_m}^{\infty} k^{-5/3} dk \right]^{1/2} \sim (k_m)^{-1/3} \sim \Delta^{1/3}. \quad (45)$$

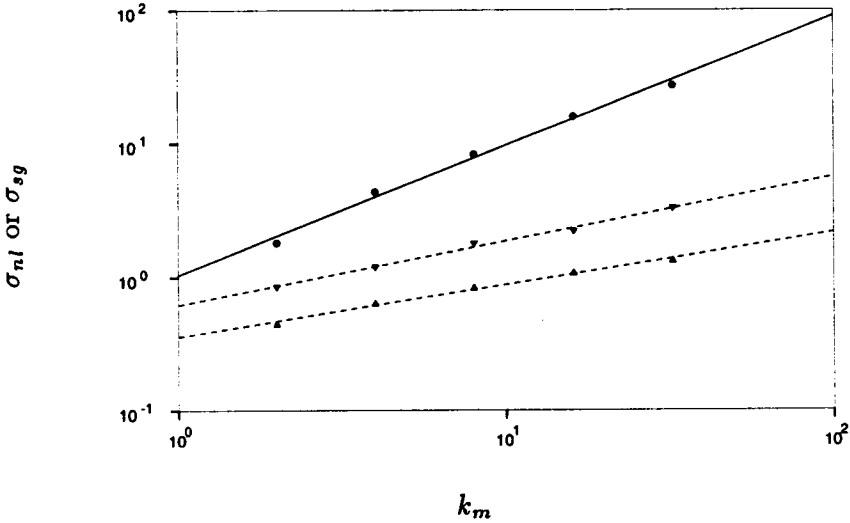


FIGURE 6. Global measure of the total nonlinear term, σ_{nl} (\bullet) and subgrid force, σ_{sg} (lower bound: \blacktriangle , upper bound: \blacktriangledown) plotted as a function of the maximum resolved wavenumber, k_m . The lines represent power law fits obtained by the least-square method.

Thus, $\nu_t \sim \Delta \Delta^{1/3} \sim \Delta^{4/3}$ so that $|\tau_{ij}| \sim \sqrt{\epsilon \nu_t} \sim \Delta^{2/3}$. The subgrid force, which is the derivative of τ_{ij} should then scale as $|\tau_{ij}|/\Delta \sim \Delta^{-1/3} \sim (k_m)^{1/3}$. The scaling exponent (0.4-0.5) in (43) is reasonably close to what this rough argument predicts. It should be noted that, even though the subgrid stress decreases with increasing resolution, its derivative, the subgrid force, actually increases.

Figure 7 shows the integrated finite-differencing error, σ_{FD} , plotted against k_m . There appears to be an asymptotic approach to a power law behavior for large k_m . A least square power law fit to the last three data points gives

$$\sigma_{FD} = k_m^{0.75} \times \begin{cases} 1.03 & \text{(Order 2)} \\ 0.82 & \text{(Order 4)} \\ 0.70 & \text{(Order 6)} \\ 0.5 & \text{(Order 8)} \\ 0 & \text{(Spectral)} \end{cases} \quad (46)$$

which are shown as solid lines in Fig. 7. The subgrid terms σ_{sg} are also shown for comparison. It is significant that the exponent in the dependence of the integrated error on resolution in (46) turns out to be independent of the order of the scheme. A higher order scheme reduces the error only through a reduced prefactor multiplying the $\sim k_m^{0.75}$ term.

Figure 8 shows the integrated value of the aliasing error σ_{alias} plotted against k_m . The lines are power law fits to the data. Only the second order scheme and the pseudo-spectral scheme without dealiasing is shown. The curves for the fourth,

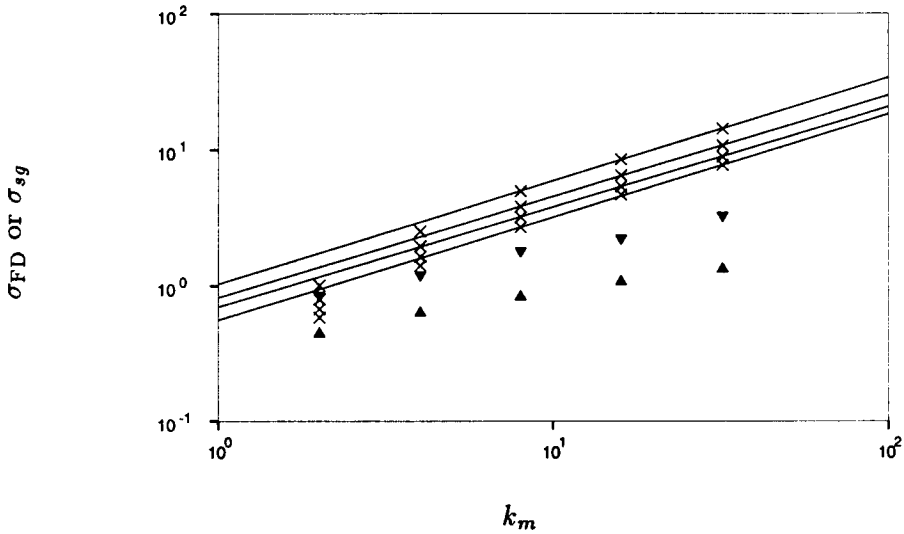


FIGURE 7. Finite-differencing errors, σ_{FD} plotted as a function of the maximum resolved wavenumber k_m (\times) for central differencing schemes of order 2 (topmost), 4, 6 and 8 (lowermost). The solid lines are least-square power law fits. Lower (\blacktriangle) and upper (\blacktriangledown) bounds of the subgrid force σ_{sg} are also shown for comparison.

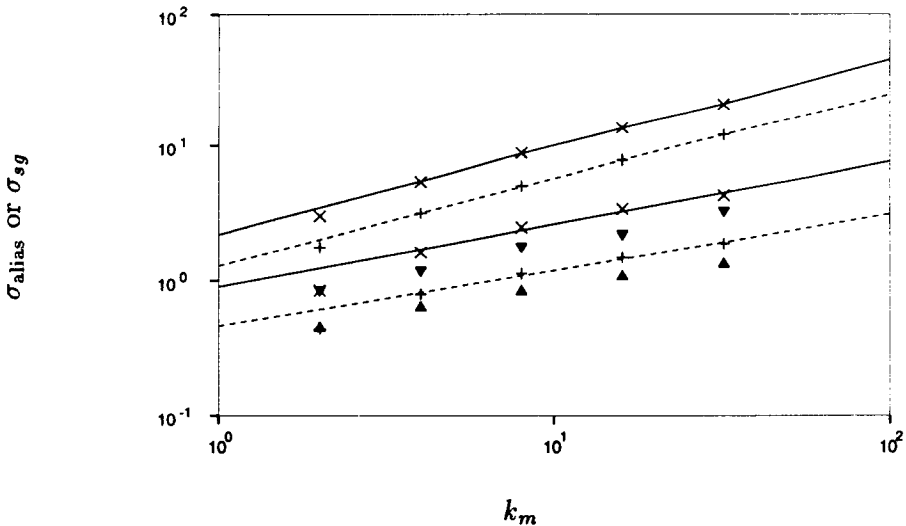


FIGURE 8. Upper and lower bounds of the aliasing error, σ_{alias} , for a second-order (+) and undealiased pseudo-spectral method (\times). Solid and dashed lines are least-square power law fits. Upper (\blacktriangledown) and lower (\blacktriangle) bounds for the subgrid term σ_{sg} are also shown for comparison.

sixth, and eighth order schemes have intermediate positions and have been omitted for clarity. These fits are given by the following analytical expressions;

$$\sigma_{\text{alias}} = \begin{cases} 0.90 k_m^{0.46} & \text{(Lower bound, Pseudo-spectral)} \\ 2.20 k_m^{0.66} & \text{(Upper bound, Pseudo-spectral)} \\ 0.46 k_m^{0.41} & \text{(Lower bound, Second-order)} \\ 1.29 k_m^{0.65} & \text{(Upper bound, Second-order)} \end{cases} \quad (47)$$

The important distinction from Fig. 7 is that here the curves are “reversed”. Thus, the lowest curve corresponds to the second order scheme and the highest corresponds to an undealiased pseudo-spectral scheme. The subgrid term σ_{sg} is also shown for comparison. Of course, for a spectral scheme properly dealiased with the ‘3/2-rule’ both the aliasing as well as the finite-differencing errors are identically zero.

2.3.3 Discussions

The results of the above analysis may be summarized as follows. In large eddy simulation, the net effect of the unresolved eddies on the resolved ones is represented by a subgrid model. The resulting equations, which are the Navier-Stokes equations augmented by an additional term, the subgrid force, is then solved numerically. In such a procedure the presumption is that the associated numerical errors are small compared to the subgrid model being used. To keep the analysis as simple as possible, isotropic turbulence in a ‘box’ with periodic boundary conditions was considered together with a simple numerical method: an order n ($n = 2$ to 8) central-difference scheme with the nonlinear term in the divergence form. It was found that the power spectrum of the aliasing error is significantly larger than the subgrid term over most of the resolved wavenumber range. Higher order schemes have the effect of increasing the aliasing error. The finite-differencing error for a second-order scheme also remains significantly larger than the subgrid term over most of the resolved wavenumber range. The situation is improved by going to higher-order schemes. However, even for an eighth-order scheme, the error dominates the subgrid term for almost half of the resolved wavenumber range. An increase in grid resolution makes the errors increase faster than the subgrid force so that the situation cannot be improved by grid refinement as long as the cut-off is in the inertial range.

We now consider a possible remedy for this difficulty. In LES the Navier-Stokes equations are first ‘filtered’ to remove all scales below some ‘filter-width’, Δ_f . The resulting equations are then discretized on a grid of spacing Δ_g . In order that the smallest resolved scales be representable on the grid, it is required that $\Delta_g \leq \Delta_f$. In practice one most often assumes $\Delta_g = \Delta_f$, to minimize computational cost and accepts the consequence that the “marginal” eddies may not be well resolved. As a matter of fact, this distinction between Δ_g and Δ_f is often ignored and one speaks of ‘filter-width’ and ‘grid-spacing’ interchangeably. However, if one expects to adequately resolve all scales up to ‘ Δ_f ’, it is natural to require that ‘ Δ_g ’ be several times smaller than ‘ Δ_f ’ (Rogallo & Moin 1984). Thus, we are led to consider an LES with a filter-width Δ_f performed on a numerical grid of spacing $\Delta_g < \Delta_f$. Clearly, in any

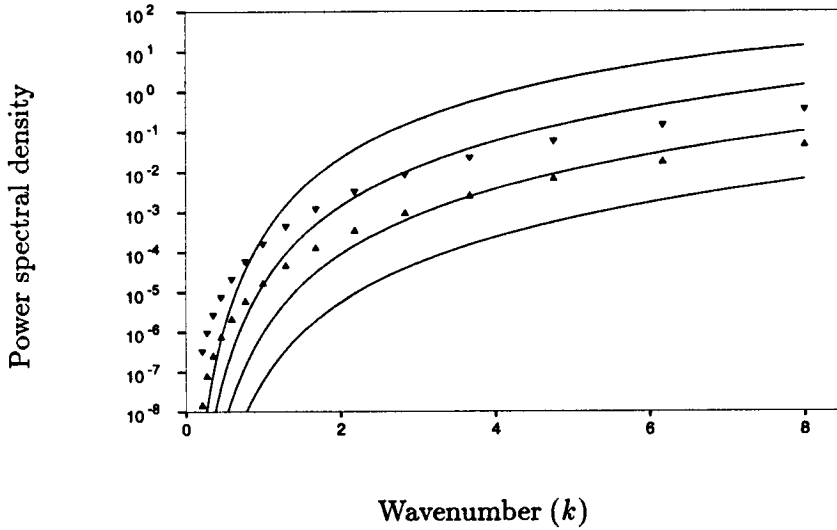


FIGURE 9. The finite-differencing error (—) for a second order central-difference scheme with $\Delta_f = N\Delta_g$ for $N = 1$ (uppermost curve), 2, 4 and 8 (lowermost curve). The lower (\blacktriangle) and upper (\blacktriangledown) bounds of the subgrid force are shown for comparison. $k_m^f = 8$ is held fixed.

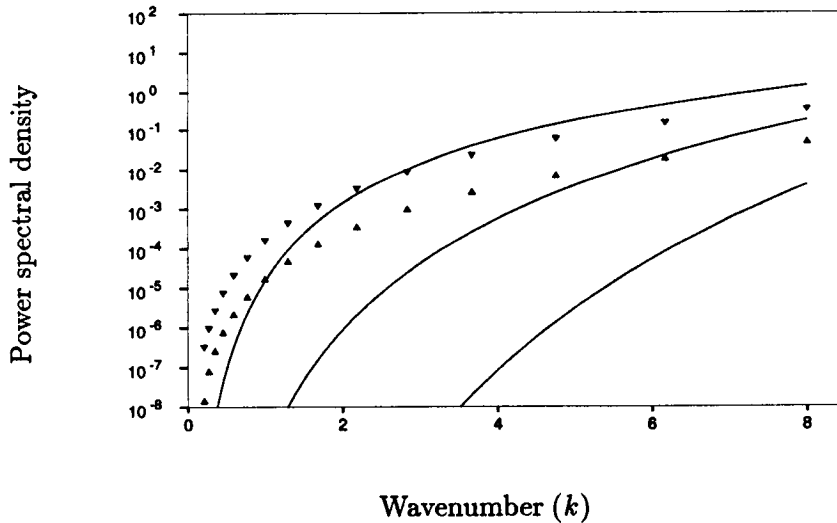


FIGURE 10. The finite-differencing error (—) for $\Delta_f = 2\Delta_g$ for a second (uppermost), fourth and eighth (lowermost) order central-difference scheme. The lower (\blacktriangle) and upper (\blacktriangledown) bounds of the subgrid force are shown for comparison. $k_m^f = 8$ is held fixed.

such computation all Fourier-modes between $k_m^f = \pi/\Delta_f$ and $k_m^g = \pi/\Delta_g$ must be held at very low amplitudes, for otherwise these “contaminated” modes would soon destroy the accuracy of computation of the modes $(0, k_m^f)$ through nonlinear interactions. This might be achieved naturally by the effective “dissipation range” of the eddy-viscosity. This may also be achieved by replacing the usual discretization of the Navier-Stokes equations by the following alternative (Lund 1995)

$$\frac{\partial u_i}{\partial t} = -\frac{\delta}{\delta x_j} \mathcal{F}[u_i u_j] - \frac{\delta \mathcal{F}[P]}{\delta x_i} - \frac{\delta \mathcal{F}[\tau_{ij}]}{\delta x_j} + \nu \frac{\delta}{\delta x_k} \frac{\delta}{\delta x_k} u_i, \quad (48)$$

where $\mathcal{F}[\]$ represents a suitably designed filtering operation that reduces the amplitudes of all modes in the range (k_m^f, k_m^g) to zero or very small values. [Compact filters for finite-difference schemes that are close to a sharp low pass filter in Fourier space were first considered by Lele (1992). They have been used in the present context by Lund (Lund 1995).] The finite-differencing operator $\delta/\delta x_j$ is on the finer grid Δ_g . The effect of this modification is easy to investigate in the present formalism. Thus, for a second order method, the ‘ Δ ’ in the expression for the modified wavenumber need simply be replaced with Δ_g . Figure 9 shows the result of such a computation for a second-order central-difference method with $\Delta_g = \Delta_f/N$ where $N = 1, 2, 4,$ and 8 for a fixed $k_m^f = 8$. It is seen that with $N = 8$, the finite-differencing error is about one or two orders of magnitude below the subgrid term throughout the wavenumber range from $k = 0$ to $k_m^f = 8$. However, taking $\Delta_g = \Delta_f/8$ increases the number of grid points by a factor of $8^3 = 512$ and the total computational cost (if the time-step, Δt is limited by the CFL condition so that $\Delta t \sim \Delta$) by a factor of $8^4 = 4096$. It may therefore be advisable to use instead a higher order scheme in conjunction with a grid that is finer than the filter-width. In Fig. 10 Δ_g has been fixed at $\Delta_f/2$ and the spectra of finite-differencing errors is plotted for a second, fourth, and eighth order scheme. It is seen that for an eighth order scheme the finite-differencing error is several orders of magnitude below the subgrid term. The increase in computational cost due to the refined grid is a factor of $2^4 = 16$. Implementation of an eighth order scheme would also carry a penalty in terms of added cost. However, in view of the vastly increased accuracy, the additional cost may be justified. In addition to reducing the finite-differencing error, the filtering scheme (48) completely removes the aliasing error. This is because modes \mathbf{k}' and \mathbf{k}'' that ‘alias’ to a mode \mathbf{k} must satisfy the relation $\mathbf{k}' + \mathbf{k}'' - \mathbf{k} = \mathbf{a}$ where \mathbf{a} is a member of the “reciprocal lattice” Λ . Any component of the vector on the left of this equation can be at most k_m^f so that the left-hand side cannot exceed $3k_m^f$. Since at least one component on the right-hand side is $2k_m^g$ or larger, the equation cannot be satisfied if $3k_m^f < 2k_m^g$, that is, if $\Delta_f > (3/2)\Delta_g$ there cannot be any aliasing errors. This is of course the well known “3/2 dealiasing rule” (see e.g. Canuto *et al.* 1988).

3. Future plans

The analysis presented in this report is kinematic in nature in the sense that the departure of the right-hand side of the Navier-Stokes operator from its ideal

value is investigated. The effect of this error on the dynamics of the solution and ultimately on the prediction of averaged quantities is unknown. However, in the light of the present findings that these errors are comparable in size to the subgrid term, a careful and systematic study is required before finite-difference methods can be considered reliable. Such a program of study should choose a specific flow for which reliable experimental data are available and for which issues such as sensitivity to initial and boundary conditions are reliably known to be unimportant. Numerical simulations should then be performed using both spectral and various finite-difference methods and the results compared to experiments and to each other. The effect of reducing errors using methods described in § 2.3.3 on relevant statistical averages should be studied.

A study of this nature has recently been undertaken by Kravchenko and Moin (Kravchenko and Moin 1995). They used a channel flow spectral code that uses B-splines in the wall normal direction and trigonometric basis functions in the homogeneous directions. By replacing the wavenumbers by the modified wavenumbers in the homogeneous directions they were able to mimic various finite difference schemes. Numerical experiments were run with various forms (divergence, rotational, skew-symmetric) of the nonlinear terms with staggered as well as nonstaggered grids. Aliasing errors in general were found to have a very serious effect on the simulation causing the flow to laminarize in some cases, as might be expected in the light of the present analysis. The effect of aliasing errors on the simulation as well as their size was found to depend strongly on both the form of the nonlinear term as well as the order of the scheme. Aliasing errors had the most serious effect for (undealiased) pseudo-spectral methods, a result also consistent with the present study. The effect of aliasing errors on numerical simulations have also been studied by Blaisdell *et al.* (1995), Zang (1991), Kim *et al.* (1987) and Moser *et al.* (1982) among others using numerical simulations.

Acknowledgments

I would like to thank Prof. Parviz Moin for encouraging me to work on this problem and for his support and constructive suggestions (in particular for suggesting the use of the Von-Karman spectrum in § 2.3). Prof. Robert Moser, Dr. Karim Shariff, Dr. Alan Wray, and Dr. Michael Rogers read the manuscript and made useful suggestions for which I am grateful. The discussion in § 2.3.3 is partly motivated by a suggestion from Dr. Thomas Lund.

REFERENCES

- BATCHELOR, G. K. 1951 Pressure fluctuations in isotropic turbulence. *Proc. Camb. Phil. Soc.* **47**, 359.
- BATCHELOR, G. K., 1953 *The theory of homogeneous turbulence*, Cambridge Univ. Press, Cambridge, England.
- BLAISDELL, G. A., SPYROPOULOS, E. T., & QIN, J. H., 1995 The effect of the formulation of nonlinear terms on aliasing errors in spectral methods. *Appl. Num. Math.* (submitted).

- CANUTO, C., HUSSAINI, M. Y., QUARTERONI, A., AND ZANG, T. A. 1988 *Spectral methods in fluid dynamics*, Springer-Verlag, Berlin.
- CHU, C. K., 1978 Numerical methods in fluid dynamics. *Advances in applied mechanics*. **18**, 285.
- GHOSAL, S. 1996 An analysis of numerical errors in large eddy simulation of turbulence. *J. Comp. Phys.* (to appear).
- HELMBERG, G., 1969 *Introduction to spectral theory in Hilbert space*, North-Holland, Amsterdam, London.
- JONES, W., & MARCH, N. H., 1973 *Theoretical solid state physics, Vol I: Perfect lattices in equilibrium*, Wiley-Interscience, London.
- KIM, J., MOIN, P. & MOSER, R. 1987 Turbulence statistics in fully developed channel flow at low Reynolds number. *J. Fluid Mech.* **192**, 365.
- KRAVCHENKO, A., & MOIN, P. 1995 On the effect of aliasing errors in spectral and finite-difference simulations of turbulent flows. (*preprint*).
- LELE, S. K. 1992 Compact finite difference schemes with spectral-like resolution. *J. Comp. Phys.* **103**, 16.
- LESIEUR, M. 1987 *Turbulence in fluids*, Kluwer Academic Publishers, Dordrecht, The Netherlands.
- LUND, T. S., 1995 (unpublished).
- MONIN, A. S. & YAGLOM, A. M. 1979 *Statistical Fluid Mechanics*, The MIT Press, Cambridge, Massachusetts.
- MOSER, R., MOIN, P., & LEONARD, A. 1982 A spectral numerical method for the Navier-Stokes equations with applications to Taylor-Couette flow. *J. Comp. Phys.* **52**, 524.
- ROGALLO, R., 1981 Numerical experiments in homogeneous turbulence. *NASA Tech. Memo. TM81315*.
- ROGALLO, R. S. & MOIN, P. 1984 Numerical simulation of turbulent flows. *Ann. Rev. Fluid Mech.* **16**, 99.
- TENNEKES, H. & LUMLEY, J. L., 1983 *A first course in turbulence*, The MIT Press, Cambridge, Massachusetts, and London, England.
- VICHNEVETSKY, R. & BOWLES, J. B. 1982 *Fourier analysis of numerical approximations of hyperbolic equations*, SIAM, Philadelphia.
- ZANG, T. A. 1991 On the rotation and skew-symmetric forms for incompressible flow simulations. *Appl. Num. Math.* **7**, 27.